

Ethyl vanillin activates TRPA1.

Shaw-wen Wu, Daniel K. Fowler, Forrest J. Shaffer, Jonathon E. M. Lindberg,
and James H. Peters

- 1- Dept. of Integrative Physiology and Neuroscience, Washington State University, Pullman, WA, USA. (DKF, FJS, JEML, JHP)
- 2- Dept. of Neuroscience, The Scripps Research Institute, Jupiter, FL, USA. (SW)

* Corresponding author.

RUNNING TITLE

EVA activates TRPA1.

CORRESPONDANCE

Shaw-wen 'Christine' Wu
Dept. of Neuroscience
The Scripps Research Institute
130 Scripps Way C349
Jupiter, FL 33458

Phone: 561-228-2000
Fax: 561-228-2341
Email: swu@scripps.edu

Text pages- 33
Tables- 0
Figures- 7
References- 52
Abstract- 250 words
Introduction- 801 words
Discussion- 1400 words

ABBREVIATIONS

AITC - Allyl isothiocyanate
CAP – capsaicin
COS-7 - CV-1 in Origin and carrying the SV40
EVA - ethyl vanillin
GFP - green fluorescent protein
KO – knock out
HEK- Human Embryonic Kidney
TRP – transient receptor potential
TRPA1 - transient receptor potential ankryn subtype family 1
TRPV1 – transient receptor potential vanilloid subtype family 1

SECTION ASSIGNMENT - Neuropharmacology

ABSTRACT

The non-selective cation channel TRPA1 is expressed in neurons of dorsal root ganglia and trigeminal ganglia and also in vagal afferent neurons that innervate the lungs and gastrointestinal tract. Many TRPA1 agonists are reactive electrophilic compounds which form covalent adducts with TRPA1. Allyl isothiocyanate (AITC), the common agonist used to identify TRPA1, contains a electrophilic group that covalently binds with cysteine residues of TRPA1 and confers a structural change on the channel. There is scientific motivation to identify additional compounds that can activate TRPA1 with different mechanisms of channel gating. We provide evidence that ethyl vanillin (EVA) is a TRPA1 agonist. Using fluorescent calcium imaging and whole-cell patch clamp electrophysiology on dissociated rat vagal afferent neurons and TRPA1 transfected COS-7 cells, we discovered that EVA activates cells also activated by AITC. Both agonists display similar current profiles and conductances. Pretreatment with A967079, a selective TRPA1 antagonist, blocks the EVA response as well as the AITC response. Furthermore, EVA does not activate vagal afferent neurons from TRPA1 knock out (KO) mice, showing selectivity for TRPA1 in this tissue. Interestingly, EVA appears to be pharmacologically different from AITC as a TRPA1 agonist. When AITC is applied before EVA, the EVA response is occluded. However, they both require intracellular oxidation in order to activate TRPA1. These findings suggest that EVA activates TRPA1 but via a distinct mechanism that may provide greater ease for study in native systems compared to AITC and may shed light on differential modes of TRPA1 gating by ligand types.

INTRODUCTION

Transient receptor potential ankyrin subtype family A 1 (TRPA1), also known as ANKTM1, is a non-selective calcium permeable cation channel found in nociceptive sensory neurons and vagal afferent neurons (Nagata et al., 2005; Story et al., 2003). TRPA1 is predominantly co-expressed with TRPV1, a heat sensitive TRP channel, in small and medium diameter sensory neurons of dorsal root ganglia (DRG) and trigeminal ganglia (TG) (Kobayashi et al., 2005; Story et al., 2003). The vagal afferent neurons that co-express TRPA1 and TRPV1 are unmyelinated C-type fibers or lightly myelinated A δ -type fibers that sense temperature, potentially initiate cardiorespiratory and gastrointestinal reflexes, and noxious stimuli to convey sensations of pain (Brierley et al., 2009; Choi et al., 2011; Fajardo et al., 2008; Hsu et al., 2013; Kobayashi et al., 2005; Lin et al., 2013; Lin et al., 2015; Liu et al., 2015; Nassenstein et al., 2008; Shen et al., 2012; Story et al., 2003; Taylor-Clark et al., 2008; Wang et al., 2013; Yu et al., 2009). Receptor co-expression has been shown via mRNA, immunohistochemistry, and treatment with agonists and antagonists in somatosensory afferents and to a lesser degree in visceral afferents (Alvarez-Berdugo et al., 2016; Chen et al., 2008; Green et al., 2016; Hondoh et al., 2010; Huang et al., 2012; Kamakura et al., 2013; Kobayashi et al., 2005; Story et al., 2003; Su et al., 2016; Weller et al., 2011; Weng et al., 2015). Originally characterized as a detector of noxious cold temperature (<17°C) (Story et al., 2003), current studies now establish that TRPA1 thermosensitivity is species specific: warm sensing in insects and cold sensing in rats and mice but unresponsive to temperature in primates (Chen and Kym, 2009; Chen et al., 2008; Gracheva et al., 2010; Sokabe et al., 2008; Viswanath et al., 2003; Zhong et al., 2012). Furthermore, TRPA1 can be manipulated to detect warmer temperatures potentially causing increasing sensitivity to heat and thermal hyperalgesia (Everaerts et al., 2011; Jabba et al., 2014; Moparthy et al., 2016).

TRPA1 is activated by many pungent compounds derived from plants such as allyl isothiocyanate (AITC), allicin, wasabi, and cinnamaldehyde (Bandell et al., 2004; Bautista et al., 2005; Jordt et al., 2004; Macpherson et al., 2007; Macpherson et al., 2005). Most TRPA1 agonists are characterized as reactive electrophiles, undergoing reversible covalent modification with cysteine and lysine residues on the ankyrin repeat domains of TRPA1 (Hinman et al., 2006; Macpherson et al., 2007). This characteristic can significantly affect TRPA1 channel gating by prolonging the open configuration of the TRPA1 channel, causing pain and neurogenic inflammation in nociceptive neurons (Bautista et al., 2006; Hinman et al., 2006; Macpherson et al., 2007; Paulsen et al., 2015). However, not all TRPA1 agonists are reactive electrophiles and some agonists are non-electrophilic, activating TRPA1 via traditional orthosteric ligand / receptor binding (Del Prete et al., 2015; Riera et al., 2009; Ryckmans et al., 2011). Thus, current efforts are underway to fully understand TRPA1 gating and synthesize or identify agonists that activate via distinct mechanisms.

Selectivity of TRP channel agonists is also important when studying TRP channels in native tissues. TRPA1 shares many agonists with TRPV3 in particular (Macpherson et al., 2006; Xu et al., 2006) including 2-APB, eugenol, carvachol, camphor, cinnamaldehyde, and vanillin (Bandell et al., 2004; Jordt et al., 2004; Lubbert et al., 2013; Macpherson et al., 2007; Macpherson et al., 2005; Macpherson et al., 2006). Ethyl vanillin (EVA), another TRPV3 agonist, is 5 to 10 times more potent compared to vanillin in terms of TRPV3 activation but its activation profile towards TRPA1 has not been explored (Xu et al., 2006). Although EVA can pharmacologically identify TRPV3, it also stimulates a large subpopulation of vagal afferent neurons in TRPV3 KO mice (Wu et al., 2016). This led us to hypothesize that EVA had additional activity at other, more abundant, TRP channels in vagal afferent neurons.

Here we provide evidence that EVA is an agonist at TRPA1. Using calcium imaging and whole-cell voltage clamp we show complete overlap of AITC and EVA sensitivity in vagal

afferent neurons and TRPA1 transfected COS-7 cells in terms of activation profiles. In addition, EVA predicts the magnitude of AITC response in vagal afferent neurons and TRPA1 transfected COS-7 cells. Pre-treatment with A967079, a selective TRPA1 antagonist, also inhibits EVA. Lastly, EVA dose-dependently stimulates dissociated neurons in rat and WT (Wu et al., 2016) but not TRPA1 KO mice. Furthermore, there are two pharmacologically distinct populations of EVA sensitive neurons where increased sensitivity to EVA also predicts sensitivity to AITC. AITC application before EVA prevents the EVA response, but not vice versa, in vagal afferent neurons and TRPA1 transfected COS-7 cells, yet they both require intracellular oxidation to induce currents. Taken together, these findings demonstrate that EVA directly stimulates TRPA1 and can identify TRPA1 in native tissues with a relatively high degree of selectivity.

MATERIALS AND METHODS

Animals.

Male Sprague Dawley rats (120-250 g, Simonsen Laboratories) and male C57BL/6 mice (20-30g) and TRPA1 KO mice (20-30 g) (B6.129P-*Trpa1tm1Kykw/J*, Jackson Laboratories) were utilized under procedures approved by the IACUC at Washington State University and in accordance with the Guide for the Care and Use of Laboratory Animals. Animals were housed under 12h light / 12h dark conditions and fed standard pellet chow *ad libitum*. Transgenic mice were genotyped using the protocol for separated PCR using primer pairs suggested by Jackson Laboratories. Genomic DNA was isolated from tail fragments using NaOH extraction. Genotyping of DNA from mouse tail fragments confirmed the identity of transgenic null mice.

Nodose ganglia isolations and primary neuronal cultures.

For primary rat and mouse neuronal cultures we removed and pooled both the left and right nodose using aseptic surgical protocols previously reported (Kinch et al., 2012). Using high-magnification and blunt dissection, the vagal trunk was dissociated from the common carotid artery. All surgeries and euthanasia were performed under a deep plane of anesthesia (Ketamine, 25 mg / 100 g; with Xylazine, 2.5 mg / 100 g). Once isolated, nodose ganglia was digested in $\text{Ca}^{2+}/\text{Mg}^{2+}$ free Hank's Balanced Salt Solution containing 1 mg/mL of both dispase II (Hoffmann- La Roche) and collagenase type 1A (Sigma-Aldrich Corp., St. Louis, MO) (90 min at 37°C in 95% air / 5% CO_2). Following enzymatic digestion the neurons were dissociated by gentle trituration through silicanized pipettes, and then washed in Dulbecco's Modified Eagle's Medium (DMEM) supplemented with 10% fetal bovine serum (FBS) and 1% penicillin-streptomycin. Dissociated neurons were plated onto poly-lysine coated coverslips maintained in

DMEM+10% FBS (37°C in 95% air / 5% CO₂) and used within 24-48 hrs of isolation for ratiometric fluorescent calcium measurements.

Molecular cloning, COS-7 cell culture, and transfection.

To generate TRPA1-GFP, the full-length mouse TRPA1 coding region (NCBI accession number NM_177781.4) without stop codon was PCR amplified from a previously generated TRPA1 expression vector using the primers below (Zhou et al., 2013) and subcloned into the KpnI and BamHI sites of pEGFP-N1 (Clontech).

Primer sequences:

5'- GGAGGGTACCGCCACCATGAAGCGCGGCTTGAGGAG-3'

5'- GAAAGGATCCCCAAAGTCCGGGTGGCTAATAGAAC-3'

Clonal COS-7 cells (ATCC[®] Manassas, VA) were plated on glass coverslips at a density of 250,000 cells per well of a 6-well tissue culture plate. HEK293 cells (ATCC[®] Manassas, VA) were plated on glass coverslips at a density of 50,000 cells per well of a 12-well plate. COS-7 and HEK293 cells were maintained in DMEM (Invitrogen), 10% FCS (Atlanta Biologicals), 25 units/ml penicillin & 25 µg/ml streptomycin (Sigma). Approximately 24 h after plating, media was replaced with DMEM, 10% FCS without pen/strep and cells were transiently transfected overnight. COS-7 cells were transfected with 2 µg of TRPA1-GFP and 2.4 µl lipofectamine 2000 (Invitrogen) per well. HEK293 cells were transfected with 1 µg of TRPA1-GFP and 1.2 µl lipofectamine 2000 per well. COS-7 cells were used for calcium imaging 16-24 hours after transfection. HEK293 cells were used for electrophysiological recordings 40-48 hours following transfection.

Ratiometric fluorescent calcium measurements.

Intracellular calcium concentrations were monitored using fluorescent Ca^{2+} indicator Fura-2 AM (Molecular Probes, Eugene, OR) on an inverted Nikon Eclipse *Ti* microscope (Nikon Instruments, Melville, NY) with an Andor Zyla digital camera (Andor Technology Ltd, Belfast, Northern Ireland). Neurons plated on coverslips the day before were loaded with Fura-2 AM (1 μM) for one hour, rinsed, and then mounted onto a closed chamber while constantly perfused with physiological bath (in mM: 140 NaCl, 5 KCl, 2 CaCl_2 , 1 MgCl_2 , 6 glucose, 10 HEPES with pH adjusted to 7.4 with Tris Base). Cells loaded with Fura-2 AM were alternatively excited with 340 and 380 nm light with fluorescence monitored at 510 nm. Data points were collected with Nikon Elements software at 6 sec time intervals and ratios of fluorescence intensity were converted to Ca^{2+} nM concentrations using a standard curve. The calcium calibration curve was determined previously using a sequential calcium titration with Fura-2 in the bath. The resulting fluorescence ratios were fit to determine the binding parameters using protocols previously summarized (Helmchen, 2011). The calibration curve is then saved in the imaging software for conversion of fluorescence ratios to calcium concentrations. Drugs were perfused via a common manifold and all manipulations were performed at room temperature. Neuron viability was confirmed through depolarization with a high potassium bath, where 55 mM KCl was used with an equimolar reduction of NaCl to 90 mM.

Whole cell patch-clamp recordings.

Recording electrodes (3 – 4.5 M Ω) were filled with CsCl internal containing (mM): 10 CsCl, 130 Cs-Methanesulfonate, 11 EGTA, 1 CaCl_2 , 1 MgCl_2 , 10 HEPES, 2 Na_2ATP , and 0.2 Na_2GTP . The intracellular solution was pH 7.4 and 285-295 mOsm. HEK293 cells were visually identified as transfected with TRPA1-GFP using an Eclipse FN1 microscope with an Intensilight C-HGFI light source filtered at 488 nm. We studied all cells under voltage clamp conditions with a MultiClamp 700B or AxoClamp 200A amplifier (Molecular Devices, Union City, CA) held initially at $V_m = -60$ mV using pipettes in whole cell patch configuration. Current-voltage relationships

were generated using a voltage step protocol: $V_{\text{hold}} = -60$ mV with 500 ms steps to -100 mV through +80 mV in 10 mV increments. Signals were filtered at 10 kHz and sampled at 30 kHz using p-Clamp software (version 10.3, Molecular Devices). Liquid junctional potentials were not corrected.

Statistical analysis.

Data for each experiment were collected from 3 or more biological replicates. When possible we designed within subject protocols and analyzed data using paired t-tests or repeated measures ANOVA followed by post-hoc comparisons against control. Linear correlations were generated with a linear regression fit regimen. Data are expressed as the average \pm SEM with all statistical analysis performed using SigmaStat software (Systat Software Inc., San Jose, CA).

Reagents

The following reagents were purchased from Sigma-Aldrich (Sigma-Aldrich, St. Louis, MO): Allyl Isothiocyanate (AITC) (#203408-Sample-K), Ethyl Vanillin (EVA) (W246409), and Capsaicin (CAP)(#M2028). A967079 (A96), a selective TRPA1 antagonist (#4716), was purchased from Tocris (Tocris, Minneapolis, MN).

RESULTS

EVA and AITC activation overlaps in vagal afferents and TRPA1 transfected COS-7 cells.

In a recent study using fluorescent calcium imaging on dissociated TRPV3 KO mouse vagal afferent neurons, we observed that EVA still activated many neurons (Wu et al., 2016), even though TRPV3 is the only reported target of EVA (Xu et al., 2006). This suggested the presence of an additional calcium influx pathway stimulated by EVA. We used calcium imaging on primary cultures of rat vagal afferent neurons (Figure 1A) and measured increases in intracellular calcium concentrations following exposure to EVA 3 mM, AITC 300 μ M, and capsaicin (CAP) 100 nM (a selective agonist for TRPV1) (Figure 1B). We calculated the percentage of cells that responded to EVA, AITC, and CAP in vagal afferent neurons for all animal subjects (Figure 1C). At these doses, we found near complete overlap of EVA and AITC sensitivity, with most of these neurons also sensitive to CAP. When EVA responses were plotted against AITC response there was a positive linear relationship (Figure 1D). The average peak EVA response was slightly but statistically larger than the average peak AITC response (Figure 1E). We considered the native co-distribution and correlated responses as consistent with EVA and AITC targeting the same receptor and very likely TRPA1. To test this hypothesis we transfected clonal COS-7 cells with full-length mouse TRPA1 C-terminally fused to GFP (TRPA1-GFP) and exposed them to EVA (3 mM) and AITC (300 μ M). EVA and AITC only activated transfected (GFP+) cells (Figure 1F), showing that wild type COS-7 cells lack endogenous TRPA1 and other potential EVA-induced calcium influx pathways such as TRPV3. GFP+ cells exhibited a similar positive relationship in the size of the calcium responses between EVA and AITC (Figure 1G). However, in the clonal cells the peak AITC response was somewhat larger than the peak EVA response (Figure 1H).

Whole cell voltage-clamp recordings of dissociated vagal afferent neurons confirmed EVA and AITC activity overlap in nodose neurons (Figure 2A); with both EVA and AITC producing strong inward currents in sensitive cells (Figure 2B). Furthermore, current-voltage (IV)

relationships revealed that EVA and AITC produced roughly the same magnitude of current in sensitive cells (Figure 2C and D) and that these curves have similar conductance in comparison to baseline (Figure 2E). Data were normalized to cell capacitance given the wide range of neuron size. Taken together, these data demonstrate that EVA has a similar conductance profile as AITC and activates an overlapping population of vagal afferent neurons.

EVA activates TRPA1.

To test the hypothesis that TRPA1 mediates the EVA response, we investigated the ability of the TRPA1 selective antagonist A967079 to eliminate EVA responses using calcium imaging. Antagonist pre-treatment eliminated the intracellular calcium influx to EVA and in some instances lowered the basal calcium level (Figure 3A); whereas, time matched control exposures to EVA did not show statistically significant agonist induced desensitization of the response (First = 85 ± 20 nM vs. 2nd = 68 ± 16 nM, N = 9 neurons, P = 0.28, paired T-test). Order of drug exposure was reversed for AITC since multiple exposures diminished the AITC induced activation (First = 130 ± 10 nM vs. 2nd = 10 ± 2 nM, N = 23 neurons, P < 0.001, paired T-test). Pretreatment with A967079 eliminated the response to AITC (Figure 3A), consistent with both agonists activating TRPA1. Summary data are quantified in Figure 3B. These experiments were replicated in COS-7 cells transfected with TRPA1-GFP (graphical data not shown). Confirming the findings in the native neurons, pretreatment with A967079 completely prevented AITC and EVA induced calcium influx in GFP+ COS-7 cells (AITC control = 105 / 123 cells, 85% response rate vs. A967079 = 0 / 78, 0% response rate; EVA control = 103 / 176, 59% response rate vs. A967079 = 0 / 83, 0% response rate). Crucially, neither EVA nor AITC activated cultured vagal afferent neurons taken from mice genetically lacking TRPA1 (TRPA1 KO), even though the neurons were shown to be viable through stimulation by CAP (100 nM) and

depolarization with elevated potassium (Hi-K) (Figure 3C-D). EVA and AITC did activate a subpopulation of vagal afferent neurons taken from wild-type mice (Figure 3E-F). Collectively, these results suggest EVA is a direct agonist of TRPA1.

Pharmacologically distinct populations of EVA-responsive vagal afferent neurons.

We exposed vagal afferent neurons to increasing concentrations of EVA to determine the activation kinetics for this agonist. While conducting this experiment we noticed that EVA responsive neurons could be grouped empirically based on the threshold concentration of EVA they responded to (Figure 4). Neurons that responded to EVA at 300 μ M or less were considered 'high' sensitivity neurons (Figure 4A, left trace); while those that required greater than 300 μ M to respond were considered 'low' sensitivity neurons (Figure 4A, right trace). These two populations of EVA sensitive neurons had distinguishable concentration-response parameters when the average response data was fit with a sigmoid function (Figure 4B). Parameters derived from these fits reveal statistically lower EC₅₀ concentrations (Figure 4C), higher average peak responses (Figure 4D), and a steeper slope, measured as power, in the linear range of the fit (Figure 4E) for the highly sensitive neurons compared to less sensitive neurons.

Extending these findings we tested concentration dependent activation with AITC with regards to high or low EVA sensitivity (Figure 5). Consistent with the EVA data, we found two populations of AITC sensitive neurons as categorized based on their sensitivity to EVA at 300 μ M. Neurons that respond to EVA at 300 μ M are also more sensitive to AITC in terms of concentration-response curves (Figure 5A, left trace), while neurons non-responsive to EVA also had smaller AITC response profiles (Figure 5A, right trace). EVA responsiveness was predictive of lower EC₅₀ and peak responses for AITC (Figure 5C and D) However, the power

between the two different populations of AITC responders was not statistically different (Figure 5E). This is distinct from EVA where the power of neurons highly sensitive to EVA is statistically lower compared to neurons that are less sensitive to EVA. These observations differentiate two distinct populations of TRPA1-containing vagal afferent neurons.

AITC masks the EVA response.

We observed that the order in which we bath applied EVA and AITC to vagal afferent neurons and TRPA1-GFP transfected COS-7 cells determined EVA sensitivity and the fidelity of EVA and AITC agonist overlap. Application of high dose EVA before application of high dose AITC (Figure 6A, left) yields high intracellular calcium responses to both agonists (Figure 6B, left) and suggests complete overlap of EVA and AITC sensitivity in rat vagal afferent neurons. However, application of AITC before EVA (Figure 6A, right) appears to prevent the subsequent EVA response yielding only high AITC intracellular calcium response and either no EVA responses or very low EVA responses (Figure 6B, right). The order in which we bath applied AITC and CAP to vagal afferent neurons (Figure 6C) did not have any effect on magnitude of AITC or CAP response (Figure 6D) suggesting the effect is specific to TRPA1. To test this phenomenon we replicated the AITC inhibition of EVA using TRPA1-GFP transfected COS-7 cells (Figure 6E-F). These data suggest EVA and AITC are both TRPA1 agonists that activate the receptor via different mechanisms such that AITC activation of TRPA1 diminishes binding or activation by EVA.

AITC and EVA induced currents are diminished by intracellular oxidative buffering. One possible difference in the mechanism of activation between AITC and EVA was the extent to which they rely on intracellular oxidation to activate the TRPA1 channel. To investigate this

possibility we recorded AITC and EVA induced whole-cell currents from TRPA1 transfected HEK293 cells with control intracellular solutions or in the presence of oxidative buffer glutathione (10 mM) (Figure 7). We found that intracellular glutathione significantly reduced the mean AITC current compared to control recordings, consistent with diminished electrophilic interactions (Figure 7A and B). The EVA induced currents were reduced to a similar extent as the AITC currents (Figure 7C and D) suggesting EVA also requires the ability to oxidize TRPA1 to activate the channel. These data suggest that differences in oxidative capacity alone do not explain differences in channel activation between AITC and EVA and might indicate additional irreversible ligand/channel interactions for AITC which EVA lacks.

DISCUSSION

The primary finding of this study is that EVA is an agonist of TRPA1 in native vagal afferent neurons and TRPA1-GFP transfected COS-7 cells with a distinct pharmacological profile from AITC. Using AITC as a reference agonist for TRPA1, we show complete overlap of AITC and EVA sensitivity in vagal afferent neurons using calcium imaging and whole-cell voltage clamp experiments. Furthermore, EVA response predicts the AITC response in vagal afferent neurons and TRPA1-GFP transfected COS-7 cells while pre-treatment with A967079, a specific TRPA1 antagonist, eliminates EVA responses. EVA dose-dependently stimulates dissociated neurons in rat and WT mice (Wu et al., 2016) but not TRPA1 KO mice. In addition, application of increasing concentrations of EVA revealed two distinct populations of EVA sensitive neurons with distinct kinetic parameters. Threshold of EVA sensitivity also predicted two distinct populations of AITC sensitive neurons with characteristic kinetic parameters. Lastly, application of AITC before EVA occludes the EVA response at a maximum concentration of 3 mM suggesting that AITC activation alters TRPA1 in such a way to prevent binding or activation by EVA. Therefore, EVA application may be useful for investigating how TRPA1 gating is differentially affected by ligand types. EVA should also be advantageous for studying TRPA1 in vagal afferent neurons and other native tissues because EVA appears to have minimal interference with TRPA1 gating; for instance, covalent modification of TRPA1 by AITC has been associated with prolonged channel activation causing tissue damage (Hinman et al., 2006; Macpherson et al., 2007).

TRP channel signaling in vagal afferent neurons.

There are a multitude of TRP channels that are expressed in vagal afferent neurons with a wide range of neurophysiological functions both in the periphery and at the central terminals (Wu et

al., 2014). However, our understanding of the actions and interactions of many of these TRP channels in the context of vagal afferent signaling is still developing. Thus far, we know that TRPV1 expression at the terminals of vagal afferent neurons contributes to asynchronous and spontaneous release of glutamate, a characteristic that enables adaptive synaptic transmission (Peters et al., 2010; Shoudai et al., 2010). TRPA1 is as abundant as TRPV1 in vagal afferent neurons and seems to co-express in TRPV1 expressing neurons (Kobayashi et al., 2005; Lin et al., 2015; Nassenstein et al., 2008), yet the role of TRPA1 in afferent neurotransmitter release is currently unexplored. In order to study the function of TRPA1 in vagal afferent signaling, we have found a way to selectively stimulate it pharmacologically in native vagal afferent neurons via EVA, which activates TRPA1 differently than the standard TRPA1 agonist AITC.

We had originally overlooked the importance of TRPA1 in vagal afferent neurons, turning our attention towards TRP channels stimulated by warm temperatures such as TRPV3. However, EVA also stimulated a significant number of vagal afferent neurons in TRPV3 KO mice demonstrating that EVA is not a selective TRPV3 agonist (Wu et al., 2016). Using a more selective TRPV3 agonist (farnesyl pyrophosphate (FPP)), we pharmacologically determined that TRPV3 was present in vagal afferent neurons in extremely small amounts (Wu et al., 2016), and therefore was likely negligible to the overall EVA response observed in wild type animals. These observations combined with our current findings suggest that EVA primarily targets TRPA1 in vagal afferent neurons. Crucially, whereas EVA concentration-dependently stimulated a sizable portion of vagal afferent neurons in TRPV3 KO mice, EVA did not stimulate any vagal afferent neurons in TRPA1 KO mice. This shows that EVA, at the concentrations used in this study, is not an agonist for any other calcium-conducting channel expressed in vagal afferent neurons. While this does not preclude EVA activity at other TRP channels, the reported expression of many TRP channels in vagal afferent neurons and lack of EVA signaling suggests a fairly high degree of specificity to TRPA1 (Buniel et al., 2004; Elg et al., 2007; Glazebrook et al., 2005;

Staaf et al., 2010; Zhang et al., 2004; Zhao et al., 2010) In TRPA1-GFP transfected COS-7 cells, we found similar overlap of EVA and AITC activation, effectiveness of TRPA1 antagonism, and linearity of fit between EVA and AITC as in native vagal afferent neurons (Figure 1). These findings strengthen the argument that EVA is an agonist of TRPA1. Our findings suggest that EVA is a selective agonist of TRPA1 in vagal afferent neurons.

Potential Importance of EVA as a TRPA1 agonist.

Many reactive compounds, similar to AITC, activate TRPA1 via covalent modification of the channel versus traditional lock and key binding. However, there are also numerous non-reactive compounds, such as menthol, that activate TRPA1 at alternative structural sites without covalently modulating the channel (Xiao et al., 2008). Despite these findings, the underlying mechanism of non-covalent TRPA1 agonism is relatively unknown. Several lines of evidence suggest that EVA is a TRPA1 agonist that activates TRPA1 differently than AITC. The chemical structure of EVA and AITC reveals that both compounds contain electrophilic nucleophile groups and intracellular buffering with glutathione (Figure 7) diminishes activation of TRPA1 by both ligands; indicating oxidation is required for increased TRPA1 gating (Materazzi et al., 2012). Yet, when AITC is applied prior to EVA it decreases the response to EVA; but EVA does not decrease the response to AITC when applied first (Figure 6). These observations suggest that EVA's mode of TRPA1 activation is in some way different than that of AITC and may suggest that AITC is a chemically more reactive nucleophile than EVA. There are several potential advantages to the differential gating kinetics of EVA activation. A less reactive nucleophile that presumably does not covalently bind to the receptor is less likely to irreversibly change channel conformation and may provide advantages from an experimental standpoint as well as perhaps in the design of compounds for potential clinical use. Our experiments involving

AITC required extended wash times to return the experimental system back to its original state. Perhaps via covalent modification of residues on the intracellular ankyrin binding domains or differential unbinding from orthosteric versus allosteric sites (Lane et al., 2013), AITC induces a change on the experimental system by keeping the TRPA1 channel in a ligand bound / open or ligand bound / inactive configuration for longer periods of time compared to EVA. As a result, EVA can be used repeatedly and requires shorter wash times. It was originally reported that vanillin, the pre-cursor to EVA, is also a TRPA1 agonist and to a small extent TRPV1 agonist (Lubbert et al., 2013). In contrast to vanillin, EVA does not appear to be a TRPV1 agonist at the concentrations we tested since it had no effect in neurons from TRPA1 KO mice which maintained their expression of TRPV1 (Figure 3). Furthermore, the differences in pharmacology between AITC and vanillin have largely not been explored. Concentration-response curves of EVA and AITC reveal that there are two distinct populations of sensitive cells with distinct magnitudes of EC_{50} , peak response, and power. These different populations may be a consequence of differential expression of TRPA1b, a TRPA1 splice variant. However, TRPA1b is not reported to be expressed in the rat nor alter the EC_{50} of AITC activation (Zhou et al., 2013). The difference may also arise as a product of TRPA1 expression level. More specifically, one would predict that large amounts of TRPA1 would exhibit a lower EC_{50} and increased apparent sensitivity to agonists compared to cells with lower amounts of TRPA1. Alternatively, additional TRP channels capable of modifying the activity of TRPA1 may be present (Everaerts et al., 2011; Hondoh et al., 2010; Huang et al., 2012; Lin et al., 2015; Lubbert et al., 2013; Weller et al., 2011; Weng et al., 2015; Wu et al., 2014). While we identified pharmacological subpopulations of EVA and AITC sensitive vagal afferents, the extent to which these differences in signaling have physiological importance is unknown.

Summary and Perspectives.

The largely non-selective profile of many TRP channel agonists and antagonists make it difficult to identify and manipulate specific TRP channels in native tissue. In this study we were able to pharmacologically identify TRPA1 using AITC and characterize the novel agonist EVA. AITC and EVA shared similarities in terms of overlap, response rate, and conductance profiles. But key differences in their chemical structures may explain differences in their activation of TRPA1; perhaps via differences in binding sites and / or affinity. EVA behaves as a low affinity full agonist compared to AITC and may provide certain advantages for experimental interrogation of TRPA1.

ACKNOWLEDGMENTS

We would like to kindly acknowledge BreeAnne Peterson for her assistance in completing this manuscript.

AUTHORSHIP CONTRIBUTIONS

Participated in research design: Wu, Fowler, and Peters

Conducted experiments: Wu, Fowler, Shaffer, Lindberg, and Peters

Performed data analysis: Wu, Fowler, Shaffer, Lindberg, and Peters

Wrote or contributed to the writing of the manuscript: Wu, Fowler, and Peters

REFERENCES

- Alvarez-Berdugo, D., Rofes, L., Farre, R., Casamitjana, J.F., Enrique, A., Chamizo, J., Padron, A., Navarro, X., and Clave, P. (2016). Localization and expression of TRPV1 and TRPA1 in the human oropharynx and larynx. *Neurogastroenterol Motil* 28, 91-100.
- Bandell, M., Story, G.M., Hwang, S.W., Viswanath, V., Eid, S.R., Petrus, M.J., Earley, T.J., and Patapoutian, A. (2004). Noxious cold ion channel TRPA1 is activated by pungent compounds and bradykinin. *Neuron* 41, 849-857.
- Bautista, D.M., Jordt, S.E., Nikai, T., Tsuruda, P.R., Read, A.J., Poblete, J., Yamoah, E.N., Basbaum, A.I., and Julius, D. (2006). TRPA1 mediates the inflammatory actions of environmental irritants and proalgesic agents. *Cell* 124, 1269-1282.
- Bautista, D.M., Movahed, P., Hinman, A., Axelsson, H.E., Sterner, O., Hogestatt, E.D., Julius, D., Jordt, S.E., and Zygmunt, P.M. (2005). Pungent products from garlic activate the sensory ion channel TRPA1. *Proc Natl Acad Sci U S A* 102, 12248-12252.
- Brierley, S.M., Hughes, P.A., Page, A.J., Kwan, K.Y., Martin, C.M., O'Donnell, T.A., Cooper, N.J., Harrington, A.M., Adam, B., Liebrechts, T., et al. (2009). The ion channel TRPA1 is required for normal mechanosensation and is modulated by algesic stimuli. *Gastroenterology* 137, 2084-2095 e2083.
- Buniel, M., Wisnoskey, B., Glazebrook, P.A., Schilling, W.P., and Kunze, D.L. (2004). Distribution of TRPC channels in a visceral sensory pathway. *Novartis Found Symp* 258, 236-243; discussion 243-237, 263-236.
- Chen, J., and Kym, P.R. (2009). TRPA1: the species difference. *J Gen Physiol* 133, 623-625.
- Chen, J., Zhang, X.F., Kort, M.E., Huth, J.R., Sun, C., Miesbauer, L.J., Cassar, S.C., Neelands, T., Scott, V.E., Moreland, R.B., et al. (2008). Molecular determinants of species-specific activation or blockade of TRPA1 channels. *J Neurosci* 28, 5063-5071.

- Choi, M.J., Jin, Z., Park, Y.S., Rhee, Y.K., and Jin, Y.H. (2011). Transient receptor potential (TRP) A1 activated currents in TRPV1 and cholecystokinin-sensitive cranial visceral afferent neurons. *Brain Res* 1383, 36-42.
- Del Prete, D., Caprioglio, D., Appendino, G., Minassi, A., Schiano-Moriello, A., Di Marzo, V., and De Petrocellis, L. (2015). Discovery of non-electrophilic capsaicinoid-type TRPA1 ligands. *Bioorg Med Chem Lett* 25, 1009-1011.
- Elg, S., Marmigere, F., Mattsson, J.P., and Ernfors, P. (2007). Cellular subtype distribution and developmental regulation of TRPC channel members in the mouse dorsal root ganglion. *J Comp Neurol* 503, 35-46.
- Everaerts, W., Gees, M., Alpizar, Y.A., Farre, R., Leten, C., Apetrei, A., Dewachter, I., van Leuven, F., Vennekens, R., De Ridder, D., et al. (2011). The capsaicin receptor TRPV1 is a crucial mediator of the noxious effects of mustard oil. *Curr Biol* 21, 316-321.
- Fajardo, O., Meseguer, V., Belmonte, C., and Viana, F. (2008). TRPA1 channels mediate cold temperature sensing in mammalian vagal sensory neurons: pharmacological and genetic evidence. *J Neurosci* 28, 7863-7875.
- Glazebrook, P.A., Schilling, W.P., and Kunze, D.L. (2005). TRPC channels as signal transducers. *Pflugers Arch* 451, 125-130.
- Gracheva, E.O., Ingolia, N.T., Kelly, Y.M., Cordero-Morales, J.F., Hollopeter, G., Chesler, A.T., Sanchez, E.E., Perez, J.C., Weissman, J.S., and Julius, D. (2010). Molecular basis of infrared detection by snakes. *Nature* 464, 1006-1011.
- Green, D., Ruparel, S., Gao, X., Ruparel, N., Patil, M., Akopian, A., and Hargreaves, K. (2016). Central activation of TRPV1 and TRPA1 by novel endogenous agonists contributes to mechanical allodynia and thermal hyperalgesia after burn injury. *Mol Pain* 12.
- Hinman, A., Chuang, H.H., Bautista, D.M., and Julius, D. (2006). TRP channel activation by reversible covalent modification. *Proc Natl Acad Sci U S A* 103, 19564-19568.

- Hondoh, A., Ishida, Y., Ugawa, S., Ueda, T., Shibata, Y., Yamada, T., Shikano, M., Murakami, S., and Shimada, S. (2010). Distinct expression of cold receptors (TRPM8 and TRPA1) in the rat nodose-petrosal ganglion complex. *Brain Res* 1319, 60-69.
- Hsu, C.C., Lin, R.L., Lee, L.Y., and Lin, Y.S. (2013). Hydrogen sulfide induces hypersensitivity of rat capsaicin-sensitive lung vagal neurons: role of TRPA1 receptors. *Am J Physiol Regul Integr Comp Physiol* 305, R769-779.
- Huang, D., Li, S., Dhaka, A., Story, G.M., and Cao, Y.Q. (2012). Expression of the transient receptor potential channels TRPV1, TRPA1 and TRPM8 in mouse trigeminal primary afferent neurons innervating the dura. *Mol Pain* 8, 66.
- Jabba, S., Goyal, R., Sosa-Pagan, J.O., Moldenhauer, H., Wu, J., Kalmeta, B., Bandell, M., Latorre, R., Patapoutian, A., and Grandl, J. (2014). Directionality of temperature activation in mouse TRPA1 ion channel can be inverted by single-point mutations in ankyrin repeat six. *Neuron* 82, 1017-1031.
- Jordt, S.E., Bautista, D.M., Chuang, H.H., McKemy, D.D., Zygmunt, P.M., Hogestatt, E.D., Meng, I.D., and Julius, D. (2004). Mustard oils and cannabinoids excite sensory nerve fibres through the TRP channel ANKTM1. *Nature* 427, 260-265.
- Kamakura, T., Ishida, Y., Nakamura, Y., Yamada, T., Kitahara, T., Takimoto, Y., Horii, A., Uno, A., Imai, T., Okazaki, S., et al. (2013). Functional expression of TRPV1 and TRPA1 in rat vestibular ganglia. *Neurosci Lett* 552, 92-97.
- Kinch, D.C., Peters, J.H., and Simasko, S.M. (2012). Comparative Pharmacology of Cholecystokinin Induced Activation of Cultured Vagal Afferent Neurons from Rats and Mice. *Plos One* 7.
- Kobayashi, K., Fukuoka, T., Obata, K., Yamanaka, H., Dai, Y., Tokunaga, A., and Noguchi, K. (2005). Distinct expression of TRPM8, TRPA1, and TRPV1 mRNAs in rat primary afferent neurons with adelta/c-fibers and colocalization with trk receptors. *J Comp Neurol* 493, 596-606.

- Lane, J.R., Sexton, P.M., and Christopoulos, A. (2013). Bridging the gap: bitopic ligands of G-protein-coupled receptors. *Trends Pharmacol Sci* 34, 59-66.
- Lin, Y.J., Hsu, H.H., Ruan, T., and Kou, Y.R. (2013). Mediator mechanisms involved in TRPV1, TRPA1 and P2X receptor-mediated sensory transduction of pulmonary ROS by vagal lung C-fibers in rats. *Respiratory Physiology & Neurobiology* 189, 1-9.
- Lin, Y.J., Lin, R.L., Ruan, T., Khosravi, M., and Lee, L.Y. (2015). A synergistic effect of simultaneous TRPA1 and TRPV1 activations on vagal pulmonary C-fiber afferents. *J Appl Physiol* (1985) 118, 273-281.
- Liu, Z., Hu, Y., Yu, X., Xi, J., Fan, X., Tse, C.M., Myers, A.C., Pasricha, P.J., Li, X., and Yu, S. (2015). Allergen challenge sensitizes TRPA1 in vagal sensory neurons and afferent C-fiber subtypes in guinea pig esophagus. *Am J Physiol Gastrointest Liver Physiol* 308, G482-488.
- Lubbert, M., Kyereme, J., Schobel, N., Beltran, L., Wetzel, C.H., and Hatt, H. (2013). Transient Receptor Potential Channels Encode Volatile Chemicals Sensed by Rat Trigeminal Ganglion Neurons. *Plos One* 8.
- Macpherson, L.J., Dubin, A.E., Evans, M.J., Marr, F., Schultz, P.G., Cravatt, B.F., and Patapoutian, A. (2007). Noxious compounds activate TRPA1 ion channels through covalent modification of cysteines. *Nature* 445, 541-545.
- Macpherson, L.J., Geierstanger, B.H., Viswanath, V., Bandell, M., Eid, S.R., Hwang, S., and Patapoutian, A. (2005). The pungency of garlic: activation of TRPA1 and TRPV1 in response to allicin. *Curr Biol* 15, 929-934.
- Macpherson, L.J., Hwang, S.W., Miyamoto, T., Dubin, A.E., Patapoutian, A., and Story, G.M. (2006). More than cool: Promiscuous relationships of menthol and other sensory compounds. *Molecular and Cellular Neuroscience* 32, 335-343.
- Materazzi, S., Fusi, C., Benemei, S., Pedretti, P., Patacchini, R., Nilius, B., Prenen, J., Creminon, C., Geppetti, P., and Nassini, R. (2012). TRPA1 and TRPV4 mediate paclitaxel-

induced peripheral neuropathy in mice via a glutathione-sensitive mechanism. *Pflugers Arch* 463, 561-569.

Moparathi, L., Kichko, T.I., Eberhardt, M., Hogestatt, E.D., Kjellbom, P., Johanson, U., Reeh, P.W., Leffler, A., Filipovic, M.R., and Zygmunt, P.M. (2016). Human TRPA1 is a heat sensor displaying intrinsic U-shaped thermosensitivity. *Sci Rep* 6, 28763.

Nagata, K., Duggan, A., Kumar, G., and Garcia-Anoveros, J. (2005). Nociceptor and hair cell transducer properties of TRPA1, a channel for pain and hearing. *J Neurosci* 25, 4052-4061.

Nassenstein, C., Kwong, K., Taylor-Clark, T., Kollarik, M., MacGlashan, D.M., Braun, A., and Udem, B.J. (2008). Expression and function of the ion channel TRPA1 in vagal afferent nerves innervating mouse lungs. *Journal of Physiology-London* 586, 1595-1604.

Paulsen, C.E., Armache, J.P., Gao, Y., Cheng, Y., and Julius, D. (2015). Structure of the TRPA1 ion channel suggests regulatory mechanisms. *Nature* 520, 511-517.

Peters, J.H., McDougall, S.J., Fawley, J.A., Smith, S.M., and Andresen, M.C. (2010). Primary afferent activation of thermosensitive TRPV1 triggers asynchronous glutamate release at central neurons. *Neuron* 65, 657-669.

Raffai, G., Khang, G., and Vanhoutte, P.M. (2015). Vanillin and vanillin analogs relax porcine coronary and basilar arteries by inhibiting L-type Ca²⁺ channels. *J Pharmacol Exp Ther* 352, 14-22.

Riera, C.E., Menozzi-Smarrito, C., Affolter, M., Michlig, S., Munari, C., Robert, F., Vogel, H., Simon, S.A., and le Coutre, J. (2009). Compounds from Sichuan and Melegueta peppers activate, covalently and non-covalently, TRPA1 and TRPV1 channels. *Br J Pharmacol* 157, 1398-1409.

Ryckmans, T., Aubdool, A.A., Bodkin, J.V., Cox, P., Brain, S.D., Dupont, T., Fairman, E., Hashizume, Y., Ishii, N., Kato, T., et al. (2011). Design and pharmacological evaluation of PF-4840154, a non-electrophilic reference agonist of the TrpA1 channel. *Bioorganic & Medicinal Chemistry Letters* 21, 4857-4859.

- Shen, M.Y., Luo, Y.L., Yang, C.H., Ruan, T., and Lai, C.J. (2012). Hypersensitivity of lung vagal C fibers induced by acute intermittent hypoxia in rats: role of reactive oxygen species and TRPA1. *Am J Physiol Regul Integr Comp Physiol* 303, R1175-1185.
- Shoudai, K., Peters, J.H., McDougall, S.J., Fawley, J.A., and Andresen, M.C. (2010). Thermally Active TRPV1 Tonicly Drives Central Spontaneous Glutamate Release. *Journal of Neuroscience* 30, 14470-14475.
- Sokabe, T., Tsujiuchi, S., Kadowaki, T., and Tominaga, M. (2008). *Drosophila* painless is a Ca²⁺-requiring channel activated by noxious heat. *J Neurosci* 28, 9929-9938.
- Staaf, S., Franck, M.C., Marmigere, F., Mattsson, J.P., and Ernfors, P. (2010). Dynamic expression of the TRPM subgroup of ion channels in developing mouse sensory neurons. *Gene Expr Patterns* 10, 65-74.
- Story, G.M., Peier, A.M., Reeve, A.J., Eid, S.R., Mosbacher, J., Hricik, T.R., Earley, T.J., Hergarden, A.C., Andersson, D.A., Hwang, S.W., et al. (2003). ANKTM1, a TRP-like channel expressed in nociceptive neurons, is activated by cold temperatures. *Cell* 112, 819-829.
- Su, D., Zhao, H., Hu, J., Tang, D., Cui, J., Zhou, M., Yang, J., and Wang, S. (2016). TRPA1 and TRPV1 contribute to iodine antiseptics-associated pain and allergy. *EMBO Rep* 17, 1422-1430.
- Taylor-Clark, T.E., McAlexander, M.A., Nassenstein, C., Sheardown, S.A., Wilson, S., Thornton, J., Carr, M.J., and Udem, B.J. (2008). Relative contributions of TRPA1 and TRPV1 channels in the activation of vagal bronchopulmonary C-fibres by the endogenous autacoid 4-oxononanal. *Journal of Physiology-London* 586, 3447-3459.
- Viswanath, V., Story, G.M., Peier, A.M., Petrus, M.J., Lee, V.M., Hwang, S.W., Patapoutian, A., and Jegla, T. (2003). Opposite thermosensor in fruitfly and mouse. *Nature* 423, 822-823.
- Wang, S., Shi, P., and Wang, Y. (2013). TRPA1 ion channels in vagal afferent nerves contribute to ventilator-induced lung injury in a rat model. *Gen Physiol Biophys* 32, 389-394.

- Weller, K., Reeh, P.W., and Sauer, S.K. (2011). TRPV1, TRPA1, and CB1 in the isolated vagus nerve--axonal chemosensitivity and control of neuropeptide release. *Neuropeptides* 45, 391-400.
- Weng, H.J., Patel, K.N., Jeske, N.A., Bierbower, S.M., Zou, W., Tiwari, V., Zheng, Q., Tang, Z., Mo, G.C., Wang, Y., et al. (2015). Tmem100 Is a Regulator of TRPA1-TRPV1 Complex and Contributes to Persistent Pain. *Neuron* 85, 833-846.
- Wu, S.W., Fenwick, A.J., and Peters, J.H. (2014). Channeling satiation: a primer on the role of TRP channels in the control of glutamate release from vagal afferent neurons. *Physiol Behav* 136, 179-184.
- Wu, S.W., Lindberg, J.E.M., and Peters, J.H. (2016). Genetic and pharmacological evidence for low-abundance TRPV3 expression in primary vagal afferent neurons. *American Journal of Physiology-Regulatory Integrative and Comparative Physiology* 310, R794-R805.
- Xiao, B., Dubin, A.E., Bursulaya, B., Viswanath, V., Jegla, T.J., and Patapoutian, A. (2008). Identification of transmembrane domain 5 as a critical molecular determinant of menthol sensitivity in mammalian TRPA1 channels. *J Neurosci* 28, 9640-9651.
- Xu, H.X., Delling, M., Jun, J.C., and Clapham, D.E. (2006). Oregano, thyme and clove-derived flavors and skin sensitizers activate specific TRP channels. *Nature Neuroscience* 9, 628-635.
- Yu, S., Gao, G., Peterson, B.Z., and Ouyang, A. (2009). TRPA1 in mast cell activation-induced long-lasting mechanical hypersensitivity of vagal afferent C-fibers in guinea pig esophagus. *Am J Physiol Gastrointest Liver Physiol* 297, G34-42.
- Zhang, L., Jones, S., Brody, K., Costa, M., and Brookes, S.J. (2004). Thermosensitive transient receptor potential channels in vagal afferent neurons of the mouse. *Am J Physiol Gastrointest Liver Physiol* 286, G983-991.
- Zhao, H., Sprunger, L.K., and Simasko, S.M. (2010). Expression of transient receptor potential channels and two-pore potassium channels in subtypes of vagal afferent neurons in rat. *Am J Physiol Gastrointest Liver Physiol* 298, G212-221.

Zhong, L., Bellemer, A., Yan, H., Ken, H., Jessica, R., Hwang, R.Y., Pitt, G.S., and Tracey, W.D. (2012). Thermosensory and nonthermosensory isoforms of *Drosophila melanogaster* TRPA1 reveal heat-sensor domains of a thermoTRP Channel. *Cell Rep* 1, 43-55.

Zhou, Y., Suzuki, Y., Uchida, K., and Tominaga, M. (2013). Identification of a splice variant of mouse TRPA1 that regulates TRPA1 activity. *Nat Commun* 4, 2399.

FOOTNOTES

This work was supported by the National Institutes of Health National Institute of Diabetes and Digestive and Kidney Diseases [Grant DK-092651].

For reprints please contact:

James Peters

Dept. of IPN, Washington State University, 1815 Ferdinand's Lane, Pullman, WA. 99164

Email: jamespeters@vetmed.wsu.edu

FIGURE LEGENDS

Figure 1: EVA and AITC sensitivity overlap in rat vagal afferent neurons. EVA stimulates AITC sensitive vagal afferent neurons and TRPA1 transfected COS-7 cells. **A)** Fluorescent photomicrographs of cultured rat vagal afferent neurons loaded with Fura-2 AM calcium indicator dye at baseline and exposed to EVA 3 mM, AITC 300 μ M, and CAP 100 nM (White arrows = EVA, AITC, and CAP responsive neurons; Red arrows = CAP only responsive). **B)** Representative calcium traces showing response profiles of vagal afferent neurons exposed to EVA 3 mM, AITC 300 μ M, and CAP 100 nM. **C)** Histogram showing the percentage of neurons sensitive to EVA, AITC, and CAP (N = 75 neurons). **D)** Scatter plot showing the positive linear relationship between EVA and AITC calcium response (N = 44 neurons, $P < 0.0001$, $R^2 = 0.35$). **E)** Average change in calcium to EVA and AITC in responsive neurons. AITC responses were statistically smaller on average compared to EVA responses (N = 44, $P = 0.01$, paired T-test). **F)** Calcium traces from non-transfected (GFP-) and transfected (GFP+) COS-7 cells with TRPA1-GFP. EVA and AITC only activated cells containing TRPA1-GFP. **G)** Similar to nodose neurons, transfected COS-7 cells show a positive linear relationship between EVA and AITC calcium response (N = 83 cells from 3 cultures, $P < 0.0001$, $R^2 = 0.28$). **H)** Average change in calcium to EVA and AITC in transfected COS-7 cells. AITC responses were statistically larger on average compared to EVA responses (N = 83 / 3, $P < 0.001$, Wilcoxon).

Figure 2: EVA and AITC produce similar current-voltage profiles in rat vagal afferent neurons. **A)** Representative current trace of an individual neuron responsive to EVA 3 mM and AITC 300 μ M. **B)** Average current densities normalized to capacitance of EVA 3 mM and AITC 300 μ M held at -60 mV (N = 11 neurons, $P = 0.001$ and $P = 0.005$ respectively, paired T-test against baseline). **C)** Representative current-voltage (I-V) relationship curve of one cell at

baseline (a) and in response to EVA (b) and AITC (c) across voltages. **D)** Average I-V relationship curve of neurons that respond to EVA (b) and AITC (c) compared to baseline (a) showing increased inward current due to EVA and AITC exposure. (N = 11 neurons). **E)** Average conductance normalized to capacitance of all cells responsive to EVA and AITC (N = 11 neurons, P= 0.003 and P = 0.018 respectively, paired T-test against baseline). Data are expressed as average \pm SEM.

Figure 3: Pharmacological and genetic evidence that EVA is a TRPA1 agonist. Pre-treatment with the selective TRPA1 antagonist A967079 eliminates the AITC and EVA responses. **A)** Representative calcium traces comparing EVA (3 mM) and AITC (300 μ M) treatment responses before and after pretreatment with 1 μ M of A967079. **B)** Average EVA and AITC increase in cytosolic calcium before and after pretreatment with A967079. (EVA: N = 31 neurons, P < 0.001, paired T-test; AITC: N = 12 neurons, P < 0.001, paired T-test). **C-D)** EVA did not stimulate any vagal afferent neurons from TRPA1 KO mice. **C)** Representative calcium traces from TRPA1 KO mice showing lack of responses to increasing concentrations of EVA (100 μ M to 3 mM) and high dose AITC (300 μ M). **D)** Average change in intracellular calcium levels across EVA dose from all neurons. (N = 25 neurons). EVA and AITC failed to produce statistically significant changes in cytosolic calcium (EVA: P = 0.10, ANOVA and AITC: P = 0.34, T-test), whereas CAP and potassium depolarization did (CAP: P < 0.001, T-test and KCl: P < 0.001, T-test). **E)** EVA activated vagal afferent neurons taken from wild-type mice that were also activated by AITC. **F)** Average change in intracellular calcium levels across EVA dose response for activated neurons (N = 23 neurons). EVA and AITC produced statistically significant changes in cytosolic calcium (EVA: P < 0.001, ANOVA and AITC: P = 0.002, T-test), along with CAP and potassium depolarization did (CAP: P < 0.001, T-test and KCl: P < 0.001, T-test). Black lines indicate time of ligand application.

Figure 4: Two pharmacologically distinct populations of EVA reactivity in vagal afferent neurons. Distinct profiles from EVA concentration response curves suggest two functionally distinct groups of EVA responsive neurons. **A)** Representative calcium traces showing profiles of high sensitivity EVA responsive neuron (left) and a low sensitivity EVA responsive neuron (right). Neurons were grouped into the 'high sensitivity' group if they responded to 300 μ M EVA or less. **B)** EVA dose response curves between two different populations of EVA sensitive neurons (dark circles: highly sensitive neurons; open circles: less sensitive neurons) (High sensitivity, N = 32 neurons; and low sensitivity, N = 31 neurons). Group data were fit with a sigmoidal curve and the following parameters were determined. **C)** Comparison of the EC₅₀ concentrations between high and low responsive populations of EVA sensitive neurons (P < 0.001, T-test). **D)** The peak response of EVA-induced increase in cytosolic calcium (P = 0.002, T-test). **E)** The slope of the linear phase for the sigmoidal fits between groups of responsive neurons (P = 0.02, T-test).

Figure 5: Threshold EVA responsiveness predicts two populations of AITC responsive neurons. **A)** Representative calcium traces showing profiles of two distinct populations of vagal afferent neurons that respond differentially to increasing concentrations of AITC depending on their sensitivity to EVA at 300 μ M (left: responds to EVA at 300 μ M; right: does not respond to EVA at 300 μ M). **B)** AITC concentration-response curves depending on sensitivity to EVA at 300 μ M (dark circles: EVA sensitive; open circles: EVA insensitive) (EVA+, N = 48 neurons; and EVA-, N = 25 neurons). **C)** The EC₅₀ concentration between the two different populations of AITC sensitive neurons depending on sensitivity to EVA at 300 μ M was statistically different (dark column: EVA sensitive; open column: EVA insensitive) (P < 0.001, T-test). **D)** The maximum AITC-induced increase in cytosolic calcium between two different populations of

neurons depending on EVA sensitivity ($P = 0.008$, T-test). **E**) The slope of the linear phase in the sigmoid fit was not statistically different between the two AITC responsive populations ($P = 0.39$, T-test).

Figure 6: AITC masks the response to EVA. When AITC is applied first the subsequent response to EVA is diminished. This does not occur to the AITC response when EVA is applied first. **A**) Representative trace of a neuron that responds to EVA (3 mM) and AITC (300 μ M) when EVA application precedes AITC (left) and when AITC application precedes EVA (right). **B**) Average AITC and EVA increases in cytosolic calcium from vagal afferents where AITC application precedes EVA ($N = 26$ neurons) and where EVA application precedes AITC ($N = 42$ neurons). AITC responses were not statistically different between the two conditions ($P = 0.45$, T-test) while EVA was significantly reduced when it followed AITC ($P < 0.001$, T-test). **C**) Representative trace of a neuron that responds to AITC 300 μ M and CAP 100 nM when AITC applications precede CAP (left trace) and when CAP application precedes AITC (right trace). **D**) Average AITC and CAP increase in cytosolic calcium from vagal afferents where AITC application precedes CAP ($N = 11$ neurons) and where CAP application precedes AITC ($N = 12$ neurons). Neither AITC ($P = 0.73$, T-test) nor the CAP ($P = 0.59$, T-test) responses were not statistically different between the two conditions. **E**) Representative EVA (3 mM) and AITC (300 μ M) response traces from TRPA1-GFP transfected COS-7 cells when EVA application precedes AITC (left) and when AITC application precedes EVA (right). **F**) Average AITC and EVA increases in cytosolic calcium from TRPA1-GFP transfected COS-7 cells where AITC application precedes EVA ($N = 125$ cells) and where EVA application precedes AITC ($N = 78$ cells). AITC responses were not statistically different between the two conditions ($P = 0.28$, Mann-Whitney) while EVA was significantly reduced when it followed AITC ($P < 0.001$, Mann-Whitney). Group data are expressed as average \pm SEM.

Figure 7: Intracellular glutathione reduces both AITC and EVA currents. AITC is known to activate TRPA1 via intracellular oxidation, however the extent to which this occurs for EVA is unknown. Here we compare the responses between standard intracellular solutions or with glutathione (10 mM) present. **A)** Representative traces showing AITC induced currents under control (left) and with intracellular glutathione (right). **B,** left panel) Average AITC induced current density from control (N = 9 cells) and glutathione groups (N = 10 cells). The presence of intracellular glutathione significantly reduced the AITC induced current (P = 0.049, T-test). **B,** right) Mean AITC currents normalized to the average control value. **C)** Representative traces showing EVA induced currents under control (left) and with intracellular glutathione (right). **D,** left panel) Average EVA induced current density from control (N = 9 cells) and glutathione groups (N = 10 cells). Intracellular glutathione significantly reduced the EVA current (P = 0.003, T-test). **D,** right panel) Mean EVA currents normalized to the average control value. Currents have been normalized to cell capacitance to control for differences in cell size.

FIGURE 1:

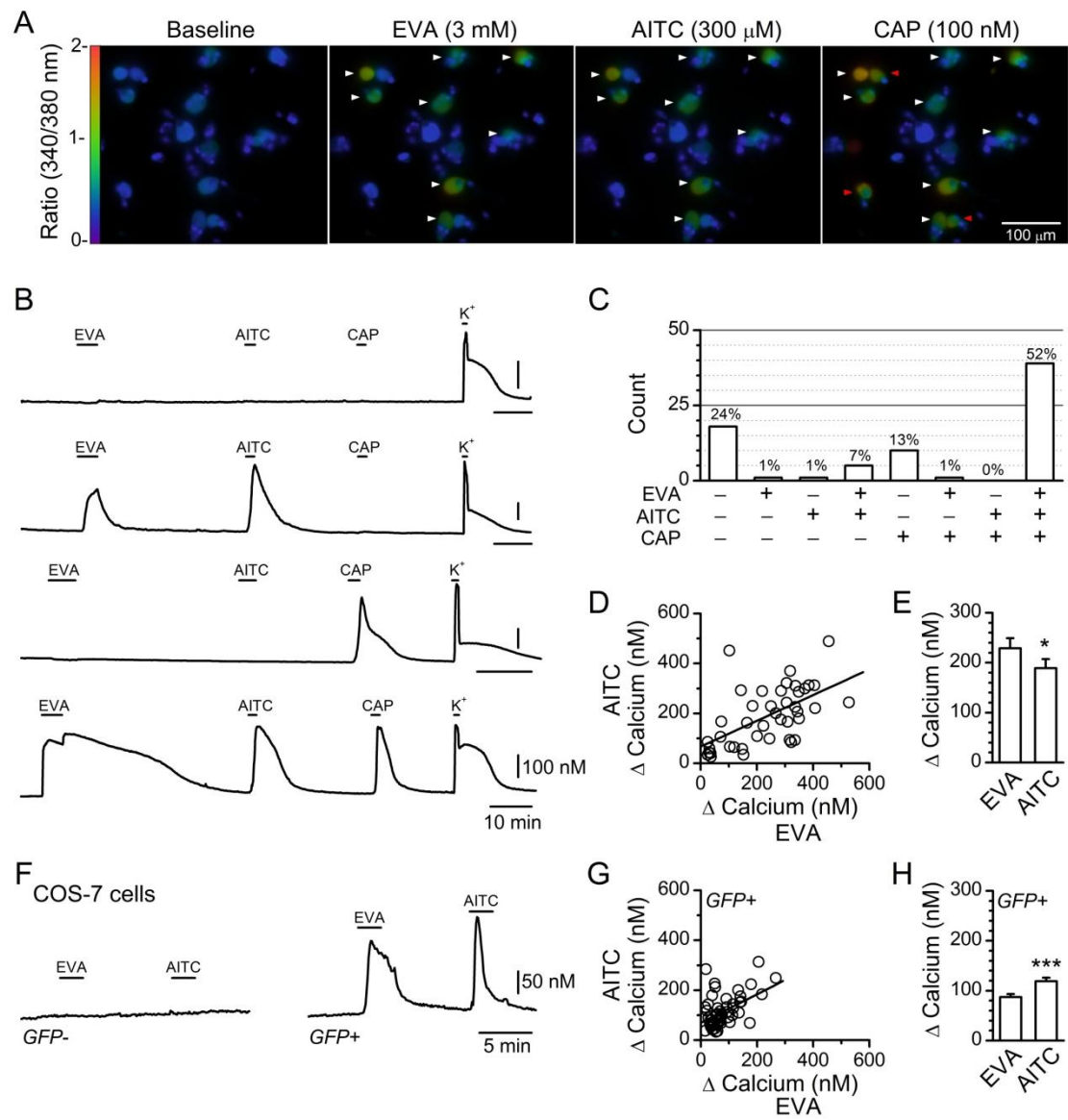


FIGURE 2:

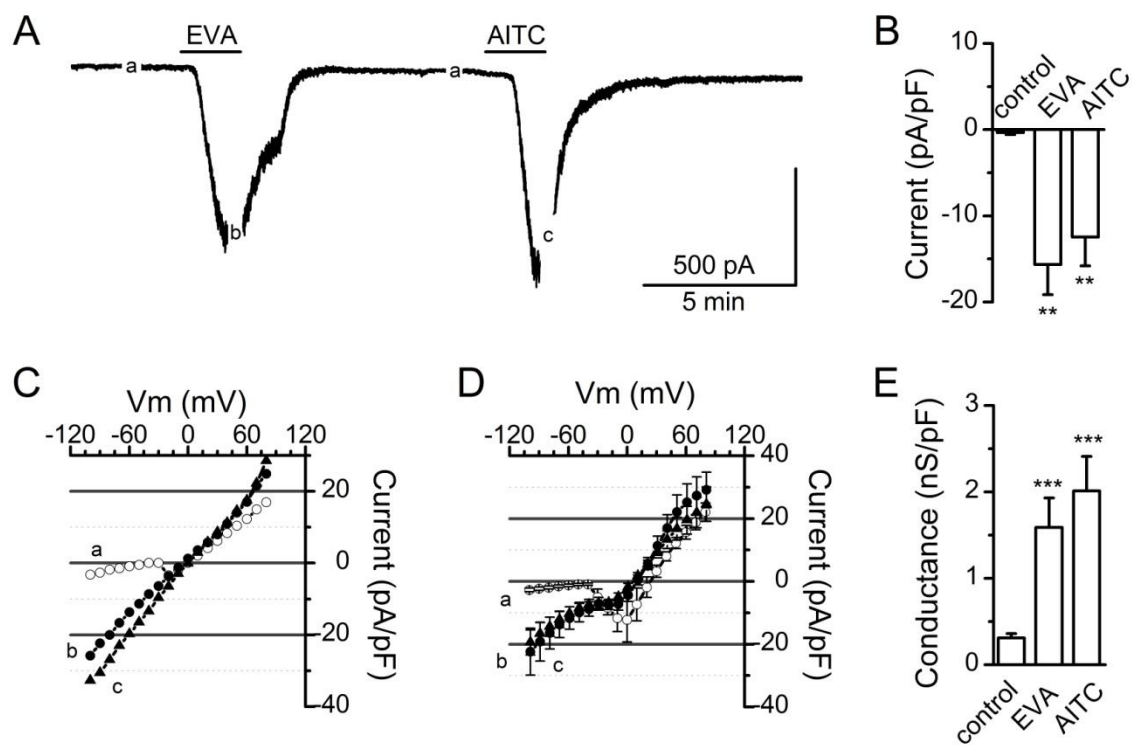


FIGURE 3:

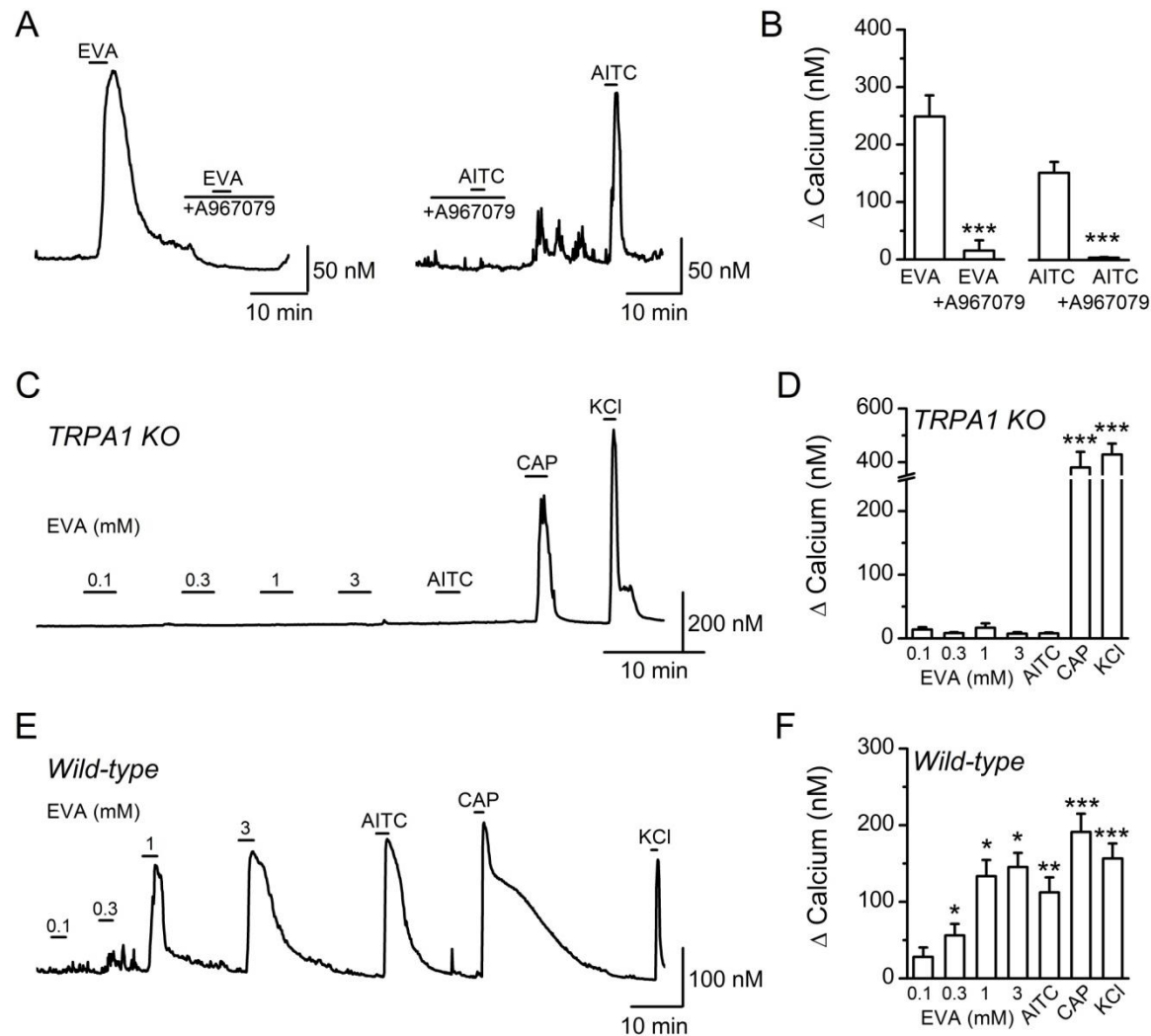


FIGURE 4:

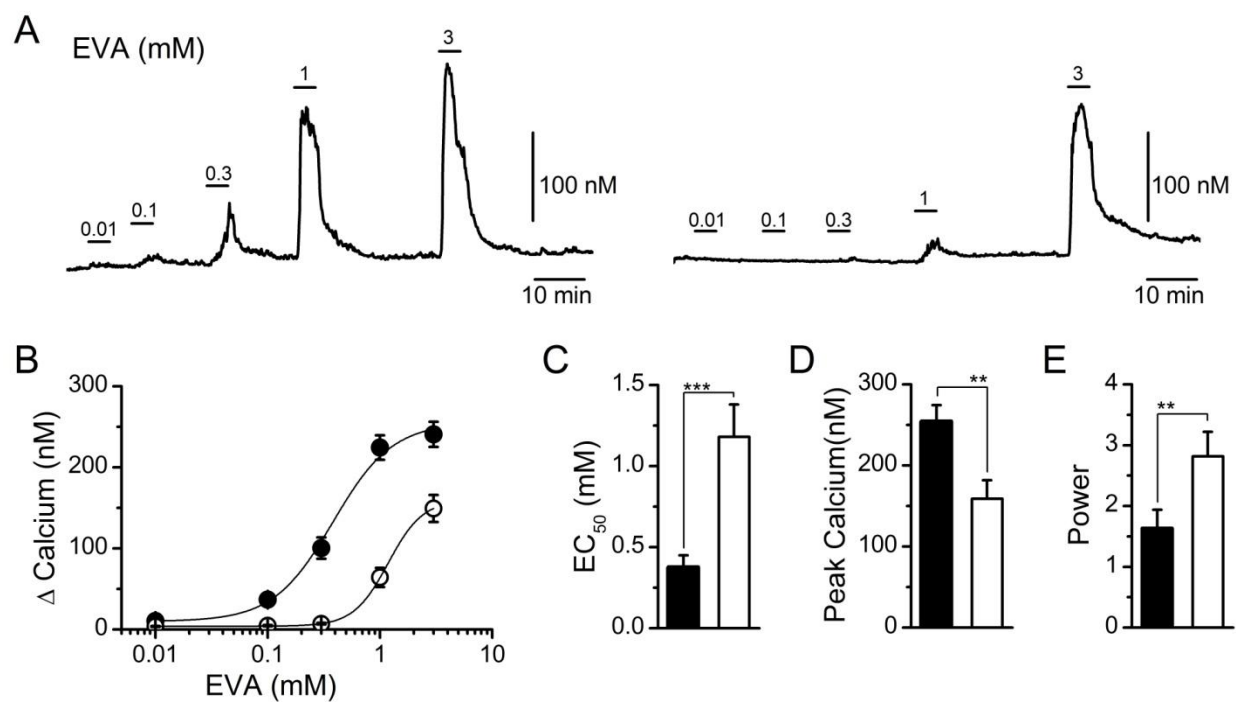


FIGURE 5:

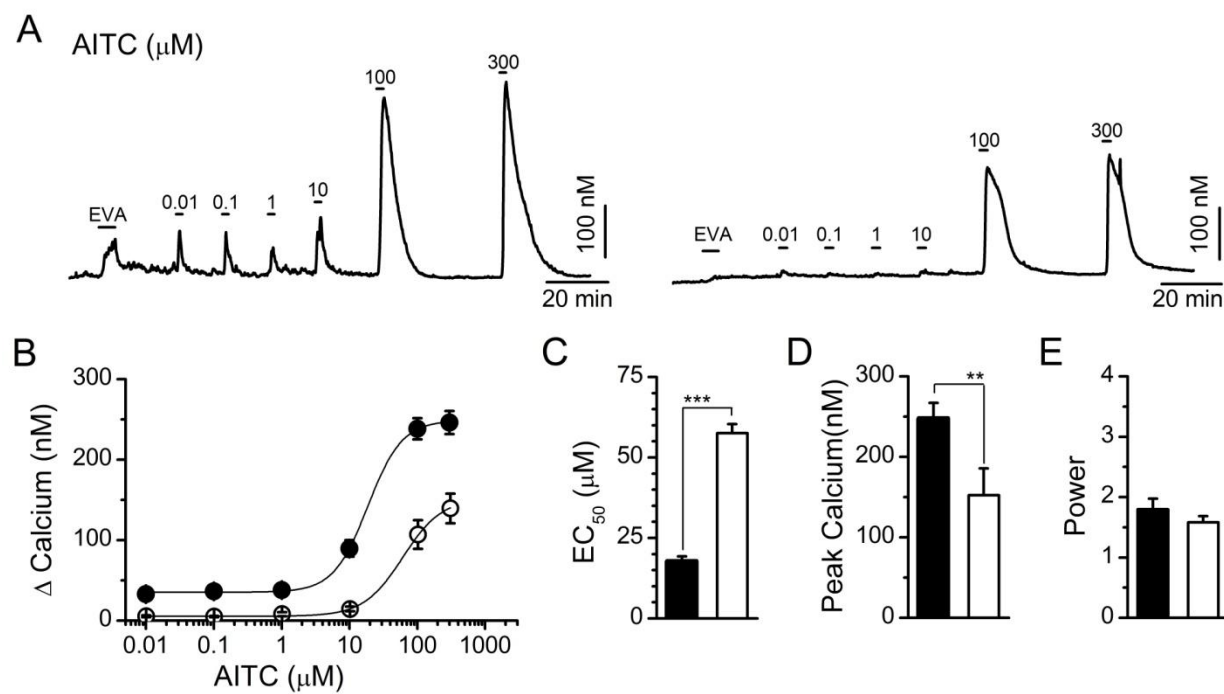


FIGURE 6:

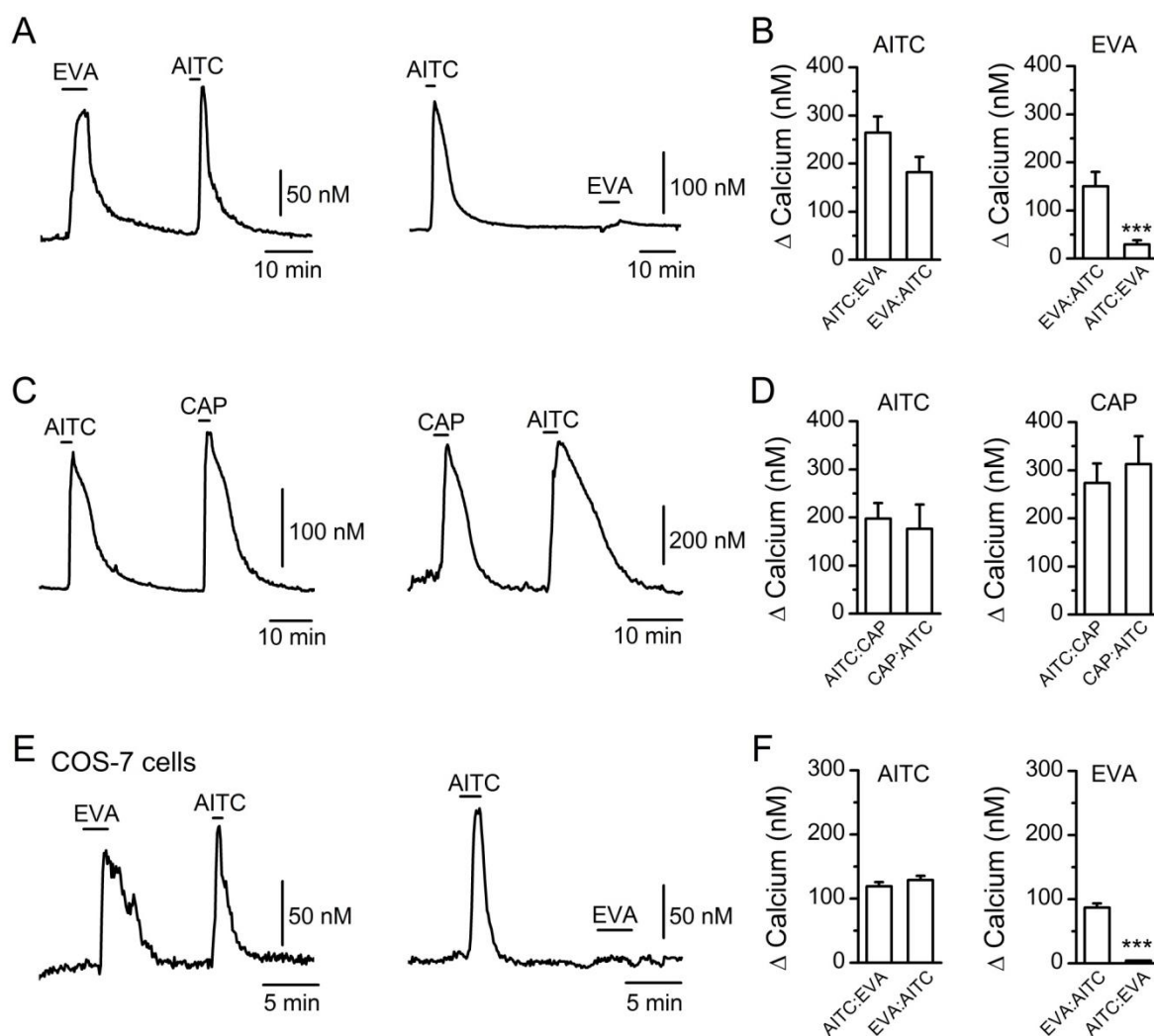


FIGURE 7:

